Green Energy and Resources 1 (2023) 100021

Contents lists available at ScienceDirect

Green Energy and Resources

journal homepage: www.journals.elsevier.com/green-energy-and-resources

Research Article

Investigation on in-situ deoxygenation performance of bio-oil model compound guaiacol over Ce-Fe/Al_2O_3 catalyst

Meiling Yang [a], Yanming Chen [a], Yong Wang [b], Laishun Yang [a], Weiwei Cui [a], Yanhui Liu [b], Cuiping Wang [a,*], Qun Chen [c]

[a] Clean Energy Lab, College of Civil Engineering and Architecture, Shandong University of Science and Technology, Shandong Province, 266590, China
[b] Qingdao DANENG Environmental Protection Equipment Incorporation Company, Shandong Province, 266300, China
[c] School of Food and Advanced Technology, Massey University, Palmerston North, 4410, New Zealand

ARTICLE INFO

Keywords:
Guaiacol
Fe-based catalyst modified by Ce
Deoxygenation
Reaction temperature
Reaction time

ABSTRACT

The investigation of the low-cost deoxygenation of guaiacol (GUA, a model bio-oil compound) is of importance for upgrading bio-oil. At present, common sulfide catalysts for GUA deoxygenation reactions cause contamination of the liquid product, and noble metal catalysts are economically disadvantageous. In this study, four reduced Fe-based oxides with different Ce doping ratios were prepared and their effects on the in-situ deoxygenation performance of GUA in aqueous/methanol hydrogen donor solvents were explored. The results based on the deoxygenation degree, conversion degree, and higher heating value (HHV) of the products showed that the oxide catalyst with a Fe/Ce molar ratio of 2:1 in the methanol solvent performed very well. After selecting an excellent catalyst and a better hydrogen donor solvent, four factors (reaction temperature, reaction time, volume ratio of GUA dosage and methanol dosage, and the ratio of catalyst dosage at the bottom of the reactor to that at the top) in the deoxygenation degree of GUA were investigated using an orthogonal experimental method to further explore the performance of the catalyst. The results showed that the reaction temperature and time greatly influenced GUA deoxygenation. Under optimal experimental conditions, the deoxygenation degree and conversion degree of GUA could reach 34.36% and 92.56%, respectively, based on the relative peak area of gas chromatography–mass spectrometry, and the HHV of the liquid product was 32.27 MJ/kg. Although Fe/Ce catalysts mainly promote demethoxylation, demethylation, and methylation, the stability and quality of the liquid products were improved compared with GUA owing to the reduction in phenolic hydroxyl and ether content. The reduced catalyst in the process of GUA in-situ deoxygenation reactions in methanol maintained a steady performance, as revealed by X-ray diffraction and X-ray fluorescence.

1. Introduction

Global energy demand is increasing annually, and bio-oil, a renewable energy source obtained from biomass pyrolysis, has wide application prospects. However, crude bio-oil has high viscosity, high acidity, and low higher heating value (HHV) (Zhang and Zhang, 2019; Hu and Gholizadeh, 2020), which hinder its industrial application as a fuel or chemical raw material. Deoxygenation is the primary method used to improve the quality of crude bio-oil (Wang et al., 2016; Hu and Gholizadeh, 2019).

Owing to the high complexity of bio-oil components, the choice of a bio-oil compound model and its deoxygenation research have become popular in recent years (Zhang et al., 2022; Si et al., 2017). Phenols are important components of bio-oil (Dang et al., 2020), and guaiacol (GUA) is apt to coke due to its difficulty of deoxygenation (Graca et al., 2013; Furimsky, 2000) and has become the most representative model for deoxygenation among phenolic compounds. Noble metal catalysts (such as Pd (Wang et al., 2020; Hong et al., 2014), Pt (Lee et al., 2016; He et al., 2018; Li et al., 2022), and Ru (Dwiatmoko et al., 2017; Ishikawa et al., 2016; Xiang et al., 2021)) and sulfide catalysts are often used to improve the deoxygenation effect of GUA. Nimmanwudipong et al. (2011) applied the prepared Pt/Al_2O_3 catalyst to the deoxygenation of GUA, which played a good catalytic role under the experimental conditions of hydrogen partial pressure of 140 KPa and conventional temperature of 300°C and demonstrated that the Lewis acid center of γ-Al_2O_3 promoted methoxy bond breaking and methyl transfer in GUA. Mukundan et al.

* Corresponding author.
E-mail address: wangcuiping@tsinghua.org.cn (C. Wang).

https://doi.org/10.1016/j.gerr.2023.100021
Received 6 March 2023; Received in revised form 10 June 2023; Accepted 11 June 2023

(2020) used reduced $CoMoS_2$/C in a high-pressure reactor (300°C, 50 bar H_2) as a deoxygenation catalyst for GUA, and observed that GUA completely reacted within 8 h, and the selectivity of deoxygenation products could reach 80% (phenol and benzene were the main products, with a selectivity of 41% and 39%, respectively). Although the above catalysts showed excellent deoxygenation effects on GUA, the noble metal catalysts are at a disadvantage in terms of economy, liquid yield, and high H_2 consumption (Raikwar et al., 2021), whereas hydrotreated products under the action of conventional sulfide catalysts are always contaminated with sulfur (Gutierrez et al., 2009). In recent years, some transition/post-transition metal-based catalysts, such as Fe (Li et al., 2022; Yan et al., 2021), Ni (Yan et al., 2021; Gutiérrez-Rubio et al., 2020; Lopez et al., 2020; Jahromi and Agblevor, 2018), and Co (Xiang et al., 2021; Laurenti et al., 2011), have been gradually used in GUA deoxygenation reactions. Olcese et al. (2013) investigated the GUA deoxygenation reaction in a fixed bed/fluidized bed and under optimal conditions (superficial gas velocity of 1.5 h^{-1}, temperature of 400°C, and H_2 partial pressure of 0.9 bar), Fe/SiO_2 catalyst converted 74% of GUA to benzene/toluene/xylene. Tian et al. (2022) tested the catalysis of NiCo/SiO_2-ZrO_2 on GUA at 240°C and 1 MPa H_2. The results revealed that GUA was completely converted, with cyclohexane selectivity of 99.9%. Owing to their low price and excellent reactivity (Chen et al., 2021; Ubando et al., 2020), Fe-based oxides are widely used in the preparation of functional particles, such as catalysts. However, their use in the GUA deoxygenation reactions without external hydrogen consumption has not yet been reported in detail. The exceptional performance of Ce oxides has a synergistic effect with Fe (Hu et al., 2018), which was investigated on Fe-based catalysts in this study.

Hydrodeoxygenation (HDO), in which hydrogen donors or zero-valent metals and water replace high-purity hydrogen, has great economic and safety benefits (da Costa et al., 2022). Tai et al. (2022) demonstrated the feasibility of in-situ HDO in a Zn-H_2O redox system for the deoxygenation of GUA. Moreover, hydrogen donor solvents can act as co-reactants in bio-oils (Oh et al., 2015). Jin et al. (2021) found that H_2-free HDO processes could be achieved using H_2O as the reaction medium in a GUA upgrading system. Free radicals, such as $-C_3H_5$ and –H, released by isopropanol, which were selected as the hydrogen donor during the pyrolysis process, play an important role in GUA deoxygenation (Fan et al., 2020). Therefore, both H_2O and alcohol can break their O-H bonds to form free hydrogen as internal hydrogen donors for GUA deoxygenation.

This study aims to find an economical and efficient way to upgrade bio-oil models in-situ. Using GUA as the bio-oil model, Ce-modified Fe_3O_4 as the catalyst, and deionized water and methanol as hydrogen donors, the deoxygenation reactions of GUA were carried out in a high-pressure reactor. There was no external hydrogen or expensive metal catalyst consumption during the GUA deoxygenation reaction, and the catalyst particles were placed in the upper and lower layers to ensure a sufficient touch reaction between the liquid–solid and GUA vapor–solid. Water solvent experiments were used for the primary understanding of the in-situ hydrogenation mechanism and for the determination of the Ce/Fe ratio range in the catalyst. Furthermore, the methanol solvent was used for a higher degree of deoxygenation and the application of the deoxygenation mechanism. The degree of deoxygenation and HHV of the liquid products are the main evaluation indices for the reactions.

2. Material and methods

2.1. Reduced deoxygenation catalysts preparation

Ceramic particles loaded with Fe/Ce at molar ratios of 1:0, 1:1, 2:1, and 3:1 were prepared by the impregnation method and were named Fe_1Ce_0/Al_2O_3, Fe_1Ce_1/Al_2O_3, Fe_2Ce_1/Al_2O_3, and Fe_3Ce_1/Al_2O_3, respectively. Fig. 1 shows the preparation of the deoxygenated catalysts. The preparation materials and catalyst dosages are listed in Table S1. A metal salt solution was prepared using Fe $(NO_3)_3{\cdot}9H_2O$ (Tianjin Damao, 98.5%) and Ce $(NO_3)_3{\cdot}6H_2O$ (Shanghai MacLean, 99.5%). A ceramic pellet (particle size 1–2 mm; the main component is Al_2O_3) was soaked in the solution for 12 h. After being filtered by a vacuum suction pump for 2 h at −0.1 MPa, the pellet was completely impregnated with the solution, transferred to a 105°C drying box, and baked until the sample weight was constant, followed by calcination at 800°C for 4 h in the muffle furnace. After cooling to room temperature, the sample was reduced in a tubular furnace with an atmosphere of 5% H_2/95% N_2 at 550°C for 4 h.

2.2. Experimental procedures

The deoxygenation experiment was performed in a high-pressure reactor (TCFYF-3, Jiangsu, China) and characterized using gas chromatography–mass spectrometry (GC–MS), Gas chromatograph (GC), X-ray diffraction (XRD), X-ray fluorescence (XRF) and calorimetry. Fig. 2 shows a schematic diagram.

First, the 8 ± 0.05 g catalyst was placed in a barbed wire mesh bag and fixed on the reactor agitator in order to keep it in full contact with GUA vapor. In addition, 2 ± 0.05 g deoxygenation catalyst was placed at the bottom of the reactor to ensure the catalyst particles touched the GUA liquid.

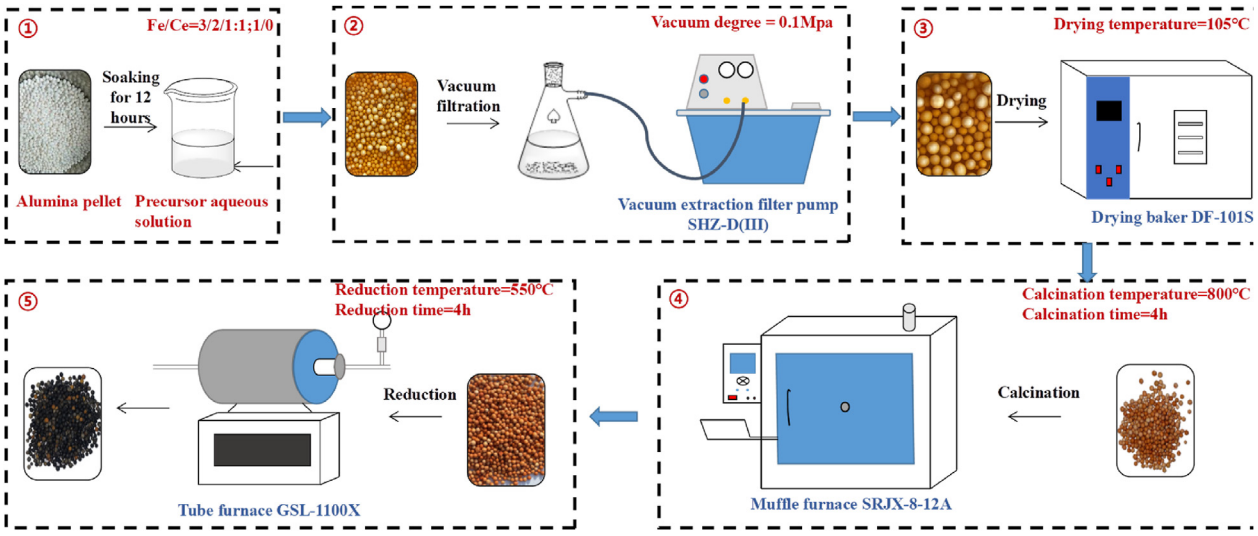

Fig. 1. Schematic diagram of catalyst preparation procedures.

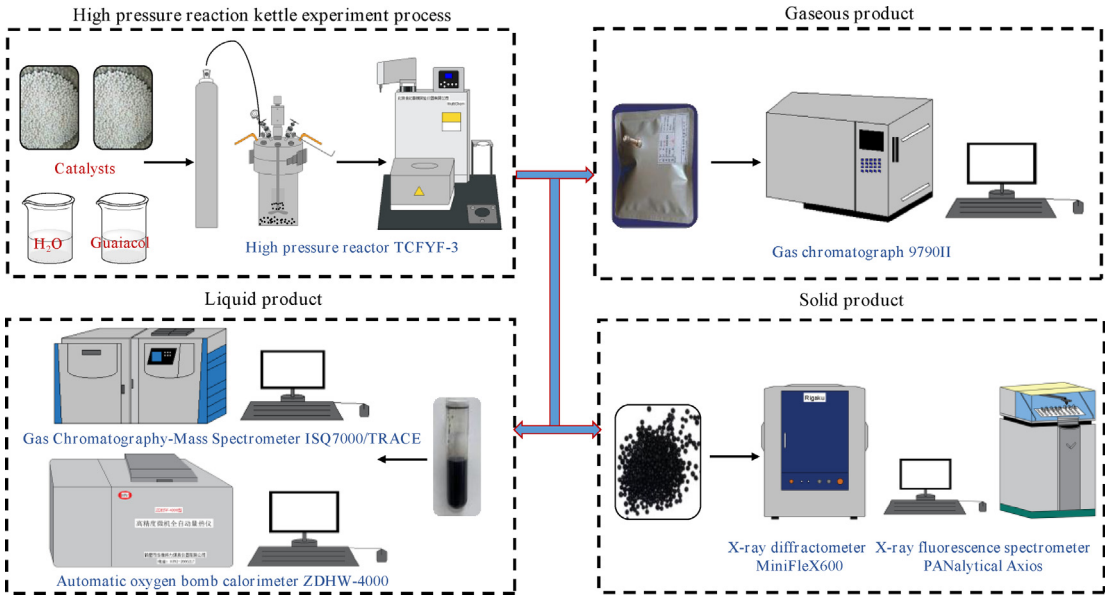

Fig. 2. Schematic diagram of experimental procedures.

Thereafter, 5 mL of GUA (Shanghai Maclean, 99.0%), and 10 mL of H_2O/methanol (Tianjin Fuyu, 99.5%) were poured into the bottom of the reactor. The reactor (250 mL in volume) was assembled and flushed with N_2 three times to remove the residual O_2 in the reactor and check gas tightness.

Finally, the reactor was heated to 350°C and kept for 30 min (Zhang et al., 2021). Thereafter, the reactor was allowed to cool naturally to room temperature. The non-condensable gas and solid products were collected directly, and the liquid products were extracted by cleaning the reactor wall and the catalyst with dichloromethane (Tianjin Yongda, 99.5%) three times. The liquid products were heated to evaporate in the rotary evaporator (RE-52, Shanghai) at 45°C to ensure the complete removal of dichloromethane until the weight of the liquid products was constant.

The orthogonal experimental method can accurately and efficiently realize a multifactorial investigation of the GUA deoxygenation reaction and determine the experimental significance and optimal combination of the involved factors (Jin et al., 2021). In this study, the reaction temperature, reaction time, ratio of catalyst dosage at the bottom to that at the top (the total catalyst mass was maintained at 10 g), and ratio of GUA to methanol dosage were selected as influencing factors to evaluate the GUA deoxygenation reactions. The orthogonal experimental design was based on the typical orthogonal test array L9 (4^3). Table S2 lists the factors and levels. The analysis of the influence laws $K_{i,j}$, and range R_i is as follows:

$$K_{i,j} = \left(\sum_{n-1}^{3} \alpha\right) \Big/ 3 \tag{1}$$

$$R_i = max\left(K_{i,j}\right) - min\left(K_{i,j}\right) \tag{2}$$

where $K_{i,j}$ represents the value of index α containing a factor, and the range R_i refers to the difference between the maximal and minimal values of the calculation results (Jin et al., 2021).

2.3. Characterization methods

The pyrolysis gas was analyzed using a gas chromatography (GC; 9790II, Fuli, China) equipped with a flame ionization detector for N_2, H_2, CO, CO_2, and CH_4.

The crystallographic structure of freshly treated oxygen carriers (OC) was evaluated using an X-ray diffractometer (MiniFlex600, Tokyo, Japan) equipped with a Cu anode at 40 kV and 15 mA. Peak intensities were recorded every 0.01° at a sweep rate of 2°/min in the range of 20~80°.

X-ray fluorescence (XRF) spectrometry has wide applications in the identification of chemical elements ranging from sodium to uranium in the materials studied. Therefore, an XRF spectrometer (PANalytical Axios, Almelo, Netherlands) was used to quantify the elemental compositions of the catalyst samples.

The carbon deposition on the catalyst surface was evaluated by a synchronous thermal analyzer (STA 449, NETZSCH), in which the reaction temperature was kept constant after heating from 35°C to 650°C. The carrier gas (N_2 or air) flow was set to 50 mL min^{-1}, and the heating rate was 20 °C·min^{-1}.

The chemical compositions of the liquid products were tested by GC–MS (Thermo Scientific, Massachusetts, United States of America). The experimental setup was the same as that previously reported (Yang et al., 2023). The conversion degree and deoxygenation degree of GUA was calculated using the following equations (Silva et al., 2021):

$$\text{conversion degree}\ (\%) = (wt_{in} - wt_{out}) / wt_{in} \times 100\% \tag{3}$$

$$\text{deoxygenation degree}\ (\%) = (wt_{O-in} - wt_{O-out}) / wt_{O-in} \times 100\% \tag{4}$$

where wt_{in} and wt_{out} represent the relative peak areas of the liquid-phase reactants and products, respectively, and $wt_{O\text{-}in}$ and $wt_{O\text{-}out}$ represent the calculated oxygen mass fractions based on the relative peak areas of the liquid phase reactants and products, respectively.

The HHV of the liquid products was measured using an automatic calorimeter (ZDHW-4000, Henan, China), and the test results were the averages of three tests.

3. Results and discussion

3.1. Effect of Ce/Fe catalyst on GUA in-situ deoxygenation reaction in the aqueous phase

Based on GC–MS analysis, the deoxygenation and conversion degrees of GUA in the aqueous phase are shown in Fig. S1. The results showed that the deoxygenation degree of GUA over Fe_2Ce_1/Al_2O_3 was the highest (5.31%), followed by 3.00% for Fe_1Ce_0/Al_2O_3 when deionized water was used as the solvent, indicating that the appropriate introduction of Ce promoted the deoxygenation of GUA. However, the conversion

degree of GUA was highest at 78.71% with Fe_1Ce_0/Al_2O_3 deoxygenation catalysts, indicating that the introduction of Ce hindered the conversion of GUA to some extent.

Fig. S2 summarizes the product distribution after GUA deoxygenation. The liquid products were predominantly benzene and phenolic compounds. Moreover, most of the organic compounds obtained in the liquid products contained a benzene ring, confirming that Fe and Ce had little effect on the hydrogenation of the benzene ring (Ubando et al., 2020). Notably, the levels of compounds containing both methoxy and hydroxyl groups in the liquid products decreased to 23.56% (Fe_1Ce_0/Al_2O_3), 40.73% (Fe_1Ce_1/Al_2O_3), 36.71% (Fe_2Ce_1/Al_2O_3), and 39.02% (Fe_3Ce_1/Al_2O_3), respectively. Therefore, the stability and quality of the liquid products were improved compared to those of GUA (Graca et al., 2013), i.e., Ce/Fe-based catalysts have a certain significance for the GUA deoxygenation reaction.

The selectivity of the catalyst for organic compounds (except GUA) based on the relative peak areas obtained by GC–MS is presented in Fig. S3. In the aqueous phase, the removal of hydroxyl groups from organic compounds was not obvious, whereas the removal of methoxy groups and transfer of methyl groups in GUA were facilitated. Liu et al. (2014) verified this result through thermodynamic and kinetic calculations. Catalysts also affected the selectivity of the liquid products. On the one hand, the catalysts showed the highest selectivity (up to 30.95%) for catechol (Fe_1Ce_0), followed by 15.40% (Fe_1Ce_1) for 2,3-dihydroxytoluene. On the other hand, except for the same organic compounds with more liquid phase products (catechol; 1,2-benzenediol, 3-methyl; -phenol; and 1,2-benzenediol, 4-methyl-), the four catalysts showed selectivity for 2-methoxy-5-methylphenol (4.25%), 2-methoxy-6-methylphenol (5.50%), 1,3-benzenediol (5.99%), and 2,5-dimethyl- (5.01%).

3.2. Effect of methanol on GUA deoxygenation reaction

Although Fe_1Ce_0/Al_2O_3 and Fe_2Ce_1/Al_2O_3 exhibited better catalytic effects on the GUA deoxygenation reaction in the aqueous phase, the conversion and deoxygenation degrees of GUA required further improvement. Therefore, a GUA deoxygenation experiment was performed using methanol as the hydrogen source (Asadieraghi and Daud, 2015). As shown in Fig. 3, the addition of Ce to the methanol phase had a more significant effect on the conversion of GUA. With an increase in the cerium dosage, the conversion and deoxygenation degrees of GUA showed increasing and then decreasing trends. In particular, the conversion and deoxygenation degrees of GUA reached 92.89% and 25.44%, respectively, over Fe_2Ce_1/Al_2O_3.

The component distributions of the liquid products in the methanol phase are shown in Fig. 4. The level of benzene cyclic hydroxyl group in the liquid product decreased relative to that in the aqueous phase from 67.01% to 60.62% over the catalyst Fe_2Ce_1/Al_2O_3, but the phenolic content in the liquid products was still high, indicating that the hydroxyl group in methanol could inhibit their dehydroxylation to generate aromatic hydrocarbons (Jiao et al., 2018). As shown in Fig. S4, Fe_2Ce_1/Al_2O_3 with better performance showed high selectivity for 2, 5-dimethylresorcinol (14.36%) and trimethylhydroquinone (10.06%). Similar to the catalytic mechanism in the aqueous phase, the Ce-Fe/Al_2O_3 catalysts promoted benzene cyclohydroxylation (derived from methanol) and methyl group transfer, and the removal of methoxy groups was more significant because methanol provided more active hydrogen, indicating that the deoxygenation degree of GUA in methanol was higher than that in the aqueous phase. Generally, an increase in the degree of deoxygenation macroscopically manifests as an increase in the HHV of the liquid phase. The HHVs of liquid products were 30.96 MJ/kg (Fe_1Ce_0/Al_2O_3), 29.95 MJ/kg ((Fe_1Ce_1/Al_2O_3), 31.61 MJ/kg (Fe_2Ce_1/Al_2O_3), and 31.05 MJ/kg (Fe_3Ce_1/Al_2O_3), respectively, which greatly improved compared to the HHV of GUA (24.58 MJ/kg). Additionally, the HHV of the liquid products over Fe_2Ce_1/Al_2O_3 was higher, which confirmed the higher degree of deoxygenation of GUA.

3.3. Analysis of the orthogonal test scheme

The influence laws and ranges of each factor are presented in Fig. 5 and Table 1. A greater value of $K_{i,j}$ indicates an obvious effect on the GUA deoxygenation degree; therefore, it was used to determine the optimal experimental conditions for the deoxygenation degree. The R_i was used to determine the degree of influence of each factor on the deoxygenation degree (Jin et al., 2021). According to the assessment index (conversion degree and deoxygenation degree of GUA), the extent of the influence of the four factors on the degree of deoxygenation of GUA was ranked as C (reaction temperature) >A (GUA dosage (ml): methanol dosage (ml)) >D (reaction time) >B (catalyst dosage (g) at the bottom: catalyst dosage (g) at the top). Conversely, as shown in Fig. 5(a) and (b), the deoxygenation degree and conversion degree of GUA decreased with an increase in A and a decrease in C. The GUA deoxygenation and conversion degrees first decreased and then increased with increasing D, reached their maximum at the second stage, and first remained unchanged and then increased with increasing B. In contrast, the conversion degree of GUA first increased and then decreased with an increase in B and reached its maximum at B2, as shown in Fig. 5(b). The highest index scheme (deoxygenation degree: A1 = 10 ml, B3 = 8 g, C3 = 350°C, and D2 = 30 min; and conversion degree: A1 = 10 ml, B3 = 5 g, C3 = 350°C, and D2 = 30 min) was determined. The results implied that with an increase in temperature, GUA produced a large number of free radicals, the reactivity of the organic compounds gradually increased, and they reacted with free hydrogen from the thermal decomposition of methanol with prolonged residence time. However, the synergistic effect of

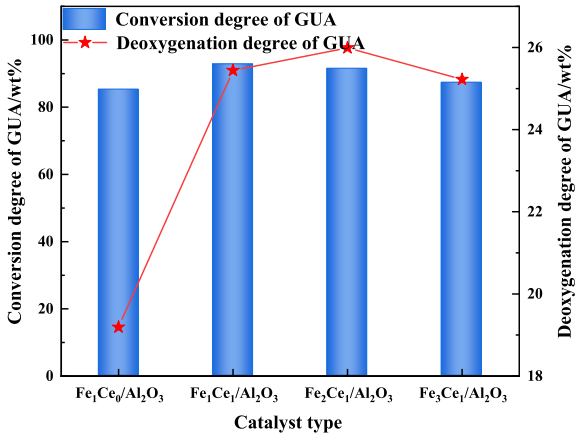

Fig. 3. GUA deoxygenation reaction over different catalysts in the methanol phase.

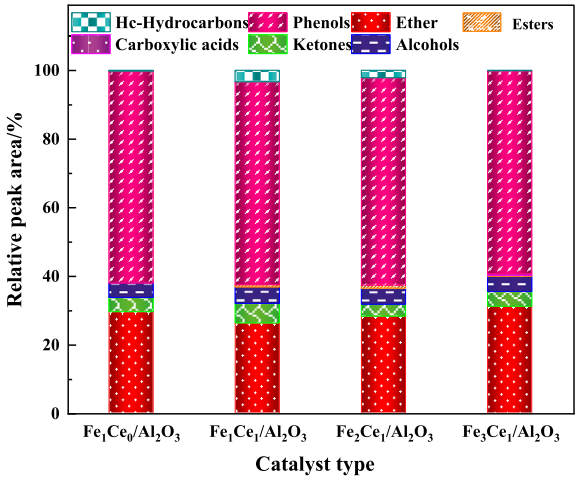

Fig. 4. Compounds distribution in the methanol phase.

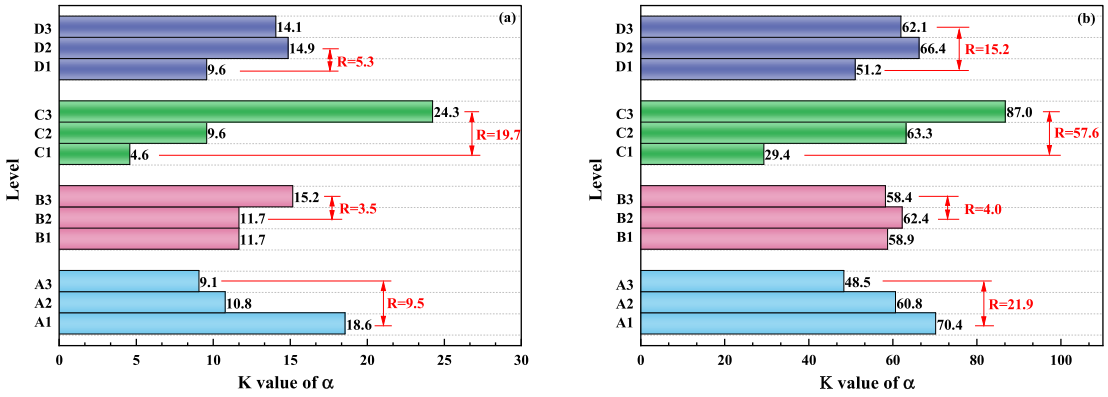

Fig. 5. The influence laws and range analysis of the (a) GUA deoxygenation degree and (b) GUA conversion degree.

Table 1
Orthogonal experimental design of GUA deoxygenation reaction.

Experimental numbers	factors			index		
	GUA dosage (ml): methanol dosage (ml)	Catalyst dosage (g) at the bottom: catalyst dosage (g) at the top	Reaction temperature (°C)	Reaction time (min)	Deoxygenation degree (%)	Conversion degree (%)
1	1:1	1:4	250	0	5.92	30.26
2	1:1	1:1	300	30	16.18	82.83
3	1:1	4:1	350	60	33.67	98.20
4	1:2	1:4	300	60	7.64	65.44
5	1:2	1:1	350	0	17.89	81.70
6	1:2	4:1	250	30	6.99	35.30
7	1:3	1:4	350	30	21.41	81.09
8	1:3	1:1	250	60	0.98	22.72
9	1:3	4:1	300	0	4.93	41.72

methanol and GUA was negatively correlated with the addition of high amounts of methanol, which might be due to the high concentration of hydroxyl groups decomposed from methanol, which inhibited the deoxygenation of GUA. Moreover, the catalyst at the bottom of the reactor still played a catalytic or oxygen-carrying role when the organic gas molecules condensed into liquid products.

Taking the degree of GUA deoxygenation as the main index, the deoxygenation of GUA under optimal conditions was verified through orthogonal experiments. As shown in Table 1, the conversion degree and deoxygenation degree of GUA were 92.56% and 34.36%, respectively, under the optimal conditions. Furthermore, the content of liquid products containing both phenolic hydroxyl groups and ether groups decreased to 25.27%, which emphasizes the need for the orthogonal experimental design method as a useful tool for selecting experimental conditions. After dichloromethane extraction, the HHV of the liquid products with good fluidity was 32.27 MJ/kg.

Based on Fig. 6, although GUA could not complete the hydrogenation of the benzene ring with the Ce-Fe/Al_2O_3 deoxygenation catalyst under optimal experimental conditions, the significant transfer of the methyl group increased the oxygen content of organic compounds, showing good selectivity for 2,3,6-trimethylphenol (13.01%) and 2,3,4,6-tetramethylphenylene (10.79%). Based on the product distribution, the possible reaction pathways for the deoxygenation of GUA are shown in Fig. 7. The liquid products obtained from the GUA under the action of the deoxygenation catalyst consisted of methoxy transfer compounds (such as 1,3-dimethoxy benzene and phenol), methyl transfer compounds (such as 2-Methoxy-6-methylphenol and 4-ethylguaiacol), and hydroxyl transfer compounds (such as hydroquinone). The Ce-Fe/Al_2O_3 catalyst mainly acted on the GUA deoxygenation through the demethoxylation (DMO), demethylation (DME), dehydroxylation, and methylation (MET) processes, which played a positive role in the removal of methoxy groups and the addition of methyl groups of GUA because the methoxy group displayed a smaller activation energy than the hydroxyl group. The methoxy groups of GUA decompose into free methyl groups and water, and the free methyl groups form CH_4 in a hydrogen atmosphere. In addition, CO_2 is produced by decarboxylation reactions, whereas CO is produced by carbonization reactions (Tran et al., 2021). Therefore, the collected non-condensable gas, though its amount was less overall, contained more CH_4 (61.99%) and H_2 (14.61%), as well as CO (9.90%) and CO_2 (11.61%). The high methane content also confirmed the release of methane when GUA methoxy groups were removed (Fig. 7), whereas the C-H bond was broken with the release of H_2 during the pyrolysis of methanol, providing a hydrogen source for GUA deoxygenation.

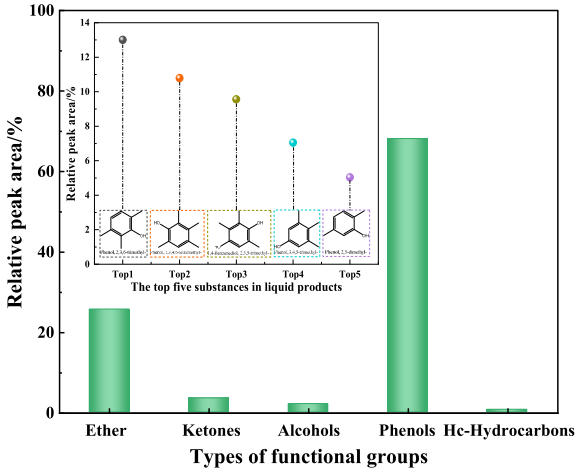

Fig. 6. Distribution of compounds and selectivity of catalysts under optimal experimental conditions.

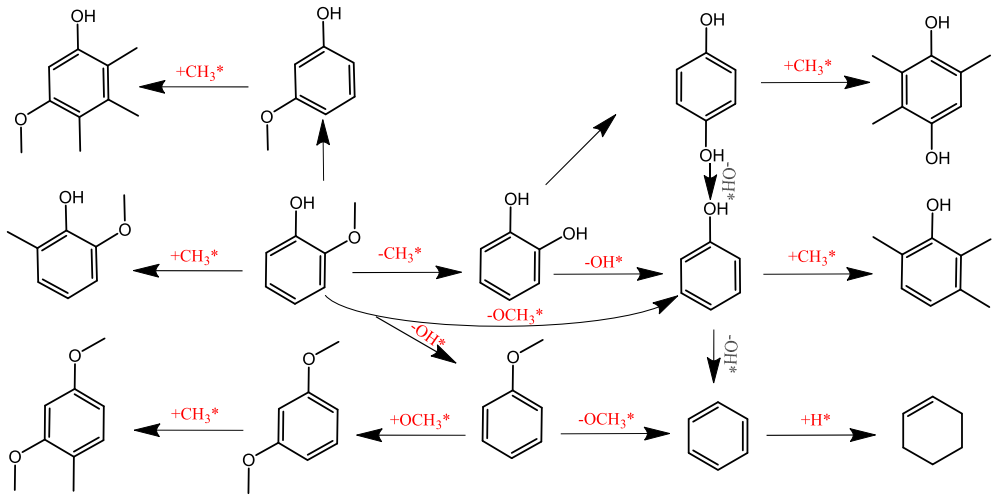

Fig. 7. Mechanism of the GUA deoxygenation reaction on the Fe_2Ce_1/Al_2O_3 catalyst under optimal experimental conditions.

3.4. Stability of Fe_2Ce_1/Al_2O_3 catalyst

The crystalline structure of the deoxygenated catalyst was characterized using XRD (Fig. 8). The peaks at 37.5°, 45.7°, and 66.6° were ascribed to the characteristic Al_2O_3 absorption peaks. The peaks at 30.4°, 35.8°, and 43.5° corresponded to the Fe_3O_4 species characteristic absorption peaks. Prominent reflections at 28.5°, 33.1°, and 47.5° associated with CeO_2 were also observed. The characteristic peaks of CeO_2 were significantly stronger than those of Fe-containing substances because not only Fe species were present in the form of Fe_3O_4 in fresh catalysts, but also the characteristic peaks of Fe_2O_3/FeO were obscured by CeO_2/Al_2O_3 or because Fe_3O_4 was well dispersed on the catalyst surface (Wang et al., 2016). XRF was used to further characterize the elemental composition of the catalyst by comparing the catalyst components before and after the reaction. There was no apparent change in the content of elements, and only the content of oxygen decreased by 0.18% (from 44.18% to 44.04%).

During the reaction in the high-pressure reactor, the organic gas molecules entering the catalyst micropores may condense with a decrease in temperature, and some can even crack, generating carbon deposits, which adversely affect the stability and activity of the catalyst (Cobella et al., 2005). For the carbon deposit check, as shown in Fig. S5, under the N_2 atmosphere and a temperature lower than 287°C, the weight loss was relatively slight, mainly due to the evaporation of bio-oil light compounds and H_2O. As the temperature increased, the heavy components continued to decompose and volatilize. After most of the organic components volatilized with a relatively flat TG curve, the atmosphere was converted into air, and the residual heavy components or low volatile compounds released flammable gases, followed by severe combustion of carbon deposits and oxidation of Fe_3O_4. During this period, the sample weight was reduced by 9.177%, showing that the carbon deposition on the surface of the catalyst was high (approximately 9.177%), which was the main cause of energy loss in the deoxygenation of GUA. Consequently, the modification of the anti-carbon deposition on the catalyst surface will be the next step in this work.

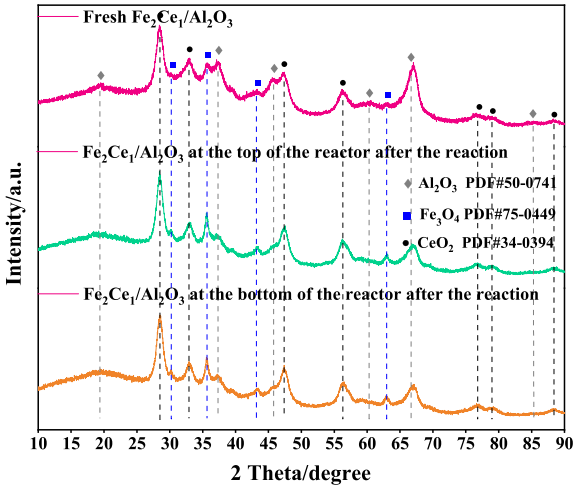

Fig. 8. XRD patterns of the Fe_2Ce_1/Al_2O_3 deoxygenation catalyst under optimal experimental conditions.

4. Conclusions

From this study, the following conclusions can be drawn for the Ce-Fe/Al_2O_3 catalyst and GUA in-situ deoxygenation reactions: (1) Out of four reduced catalysts with different Fe/Ce ratios supported by Al_2O_3 pellets prepared using the impregnation method for GUA deoxygenation in the aqueous phase, the Fe_2Ce_1/Al_2O_3 was more conducive to the deoxygenation of GUA, which was also confirmed in the methanol phase. (2) An orthogonal experiment was designed using the degree of deoxygenation of the GUA as the index. The effect of reaction temperature on the deoxygenation of GUA was the most significant. In methanol solvent, the deoxygenation degree and conversion degree of GUA under the optimal experimental conditions catalyzed by Fe_2Ce_1/Al_2O_3 reached 34.36% and 92.56%, respectively, and the responsible HHV of the liquid product was 32.27 MJ/kg, which was greatly improved compared with GUA (24.58 MJ/kg). (3) The deoxygenation of GUA over a Ce-Fe/Al_2O_3 catalyst was mainly reflected in the DMO, DME, and MET processes.

In summary, the Ce-Fe/Al_2O_3 catalyst prepared in this study performed well in the GUA deoxygenation reaction without external hydrogen, which provides guidance for improving the quality of bio-oil and the preparation of chemicals. Therefore, the research results will be advantageous for practical applications. Nevertheless, the hydrogenation capacity and carbon-deposition resistance of the catalyst must be improved.

Declaration of competing interest

The authors declare that they have no known competing financial interests or personal relationships that could have appeared to influence the work reported in this paper.

Acknowledgements

This work was supported by the National Natural Science Foundation of China (No. 52076125) and the Key Natural Science Foundation of Shandong Province (Grant No. ZR2020KE040).

Appendix A. Supplementary data

Supplementary data to this article can be found online at https://doi.org/10.1016/j.gerr.2023.100021.

References

Asadieraghi, M., Daud, W.M.A.W., 2015. In-situ catalytic upgrading of biomass pyrolysis vapor: Co-feeding with methanol in a multi-zone fixed bed reactor. Energy Convers. Manag. 92, 448–458. https://doi.org/10.1016/j.enconman.2014.12.082.

Chen, W.H., Chen, K.H., Ubando, A.T., et al., 2021. Redox degrees of iron-based oxygen carriers in cyclic chemical looping combustion using thermodynamic analysis. Chem. Eng. J. 426, 130834. https://doi.org/10.1016/j.cej.2021.130834.

Corbella, B.M., de Diego, L.F., García-Labiano, F., et al., 2005. Characterization study and five-cycle tests in a fixed-bed reactor of titania-supported nickel oxide as oxygen carriers for the chemical-looping combustion of methane. Environ. Sci. Technol. 39 (15), 5796–5803. https://doi.org/10.1021/es048015a.

da Costa, A.A.F., de Oliveira Pires, L.H., Padron, D.R., et al., 2022. Recent advances on catalytic deoxygenation of residues for bio-oil production: an overview. Mol. Catal. 518, 112052. https://doi.org/10.1016/j.mcat.2021.112052.

Dang, R., Ma, X., Luo, J., et al., 2020. Hydrodeoxygenation of 2-methoxy phenol: effects of catalysts and process parameters on conversion and products selectivity. J. Energy Inst. 93 (4), 1527–1534. https://doi.org/10.1016/j.joei.2020.01.015.

Dwiatmoko, A.A., Kim, I., Zhou, L., et al., 2017. Hydrodeoxygenation of guaiacol on tungstated zirconia supported Ru catalysts. Appl. Catal., A 543, 10–16. https://doi.org/10.1016/j.apcata.2017.05.037.

Fan, X., Wu, Y., Li, Z., et al., 2020. Benzene, toluene and xylene (BTX) from in-situ gas phase hydrodeoxygenation of guaiacol with liquid hydrogen donor over bifunctional non-noble-metal zeolite catalysts. Renew. Energy 152, 1391–1402. https://doi.org/10.1016/j.renene.2020.01.015.

Furimsky, E., 2000. Catalytic hydrodeoxygenation. Appl. Catal. 199 (2), 147–190. https://doi.org/10.1016/S0926–860X(99)00555-4.

Graca, I., Lopes, J.M., Cerqueira, H.S., et al., 2013. Bio-oils upgrading for second generation biofuels. Ind. Eng. Chem. Res. 52 (1), 275–287. https://doi.org/10.1021/ie301714x.

Gutiérrez-Rubio, S., Berenguer, A., Přech, J., et al., 2020. Guaiacol hydrodeoxygenation over Ni2P supported on 2D-zeolites. Catal. Today 345, 48–58. https://doi.org/10.1016/j.cattod.2019.11.015.

Gutierrez, A., Kaila, R.K., Honkela, M.L., et al., 2009. Hydrodeoxygenation of guaiacol on noble metal catalysts. Catal. Today 147 (3–4), 239–246. https://doi.org/10.1016/j.cattod.2008.10.037.

He, Z., Hu, M., Wang, X., 2018. Highly effective hydrodeoxygenation of guaiacol on Pt/TiO2: promoter effects. Catal. Today 302, 136–145. https://doi.org/10.1016/j.cattod.2017.02.034.

Hong, Y.K., Lee, D.W., Eom, H.J., et al., 2014. The catalytic activity of Pd/WOx/γ-Al2O3 for hydrodeoxygenation of guaiacol. Appl. Catal., B 150, 438–445. https://doi.org/10.1016/j.apcatb.2013.12.045.

Hu, X., Gholizadeh, M., 2019. Biomass pyrolysis: a review of the process development and challenges from initial researches up to the commercialization stage. J. Energy Chem. 39, 109–143. https://doi.org/10.1016/j.jechem.2019.01.024.

Hu, X., Gholizadeh, M., 2020. Progress of the applications of bio-oil. Renewable Sustainable Energy Rev. 134, 110124. https://doi.org/10.1016/j.rser.2020.110124.

Hu, Y., Jiang, G., Xu, G., et al., 2018. Hydrogenolysis of lignin model compounds into aromatics with bimetallic Ru-Ni supported onto nitrogen-doped activated carbon catalyst. Mol. Catal. 445, 316–326. https://doi.org/10.1016/j.mcat.2017.12.009.

Ishikawa, M., Tamura, M., Nakagawa, Y., et al., 2016. Demethoxylation of guaiacol and methoxybenzenes over carbon-supported Ru–Mn catalyst. Appl. Catal., B 182, 193–203. https://doi.org/10.1016/j.apcatb.2015.09.021.

Jahromi, H., Agblevor, F.A., 2018. Hydrotreating of guaiacol: a comparative study of Red mud-supported nickel and commercial Ni/SiO2-Al2O3 catalysts. Appl. Catal., A 558, 109–121. https://doi.org/10.1016/j.apcata.2018.03.016.

Jiao, Z., Wei, J., Shen, D., et al., 2018. Formation of aromatic hydrocarbons from co-pyrolysis of lignin-related model compounds with hydrogen-donor reagents. J. Anal. Appl. Pyrolysis 134. https://doi.org/10.1016/j.jaap.2018.06.002.

Jin, C., Sun, J., Chen, Y., et al., 2021a. Sawdust wastes-derived porous carbons for CO2 adsorption. Part 1. Optimization preparation via orthogonal experiment. Sep. Purif. Technol. 276, 119270. https://doi.org/10.1016/j.jece.2022.108265.

Jin, W., Pastor-Pérez, L., Villora-Picó, J.J., et al., 2021b. In-situ HDO of guaiacol over nitrogen-doped activated carbon supported nickel nanoparticles. Appl. Catal., A 620, 118033. https://doi.org/10.1016/j.apcata.2021.118033.

Laurenti, D., Afanasiev, P., Geantet, C., 2011. Hydrodeoxygenation of guaiacol with CoMo catalysts. Part I: promoting effect of cobalt on HDO selectivity and activity. Appl. Catal., B 101 (3–4), 239–245. https://doi.org/10.1016/j.apcatb.2010.10.025.

Lee, E.H., Park, R., Kim, H., et al., 2016. Hydrodeoxygenation of guaiacol over Pt loaded zeolitic materials. J. Ind. Eng. Chem. 37, 18–21. https://doi.org/10.1016/j.jiec.2016.03.019.

Li, L., Nie, X., Chen, Y., et al., 2022. Computational understanding of Fe-Pt synergy in promoting guaiacol hydrodeoxygenation. Surf. Sci. 717, 121985. https://doi.org/10.1016/j.susc.2021.121985.

Liu, C., Zhang, Y., Huang, X., 2014. Study of guaiacol pyrolysis mechanism based on density function theory. Fuel Process. Technol. 123, 159–165. https://doi.org/10.1016/j.fuproc.2014.01.002.

Lopez, M., Palacio, R., Royer, S., et al., 2020. Mesostructured CMK-3 carbon supported Ni–ZrO2 as catalysts for the hydrodeoxygenation of guaiacol. Microporous Mesoporous Mater. 292, 109694. https://doi.org/10.1016/j.micromeso.2019.109694.

Mukundan, S., Beltramini, J., Kumar, K.G., et al., 2020. Surface engineering of carbon supported CoMoS–an effective nanocatalyst for selective deoxygenation of lignin derived phenolics to arenes. Appl. Catal., A 606, 117811. https://doi.org/10.1016/j.apcata.2020.117811.

Nimmanwudipong, T., Runnebaum, R.C., Block, D.E., et al., 2011. Catalytic reactions of guaiacol: reaction network and evidence of oxygen removal in reactions with hydrogen. Catal. Lett. 141 (6), 779–783. https://doi.org/10.1007/s10562-011-0576-4.

Oh, S., Hwang, H., Choi, H.S., et al., 2015. The effects of noble metal catalysts on the bio-oil quality during the hydrodeoxygenative upgrading process. Fuel 153, 535–543. https://doi.org/10.1016/j.fuel.2015.03.030.

Olcese, R., Bettahar, M.M., Malaman, B., et al., 2013. Gas-phase hydrodeoxygenation of guaiacol over iron-based catalysts. Effect of gases composition, iron load and supports (silica and activated carbon). Appl. Catal., B 129, 528–538. https://doi.org/10.1016/j.apcatb.2012.09.043.

Raikwar, D., Majumdar, S., Shee, D., 2021. Synergistic effect of Ni-Co alloying on hydrodeoxygenation of guaiacol over Ni-Co/Al2O3 catalysts. Mol. Catal. 499, 111290. https://doi.org/10.1016/j.mcat.2020.111290.

Si, Z., Zhang, X., Wang, C., et al., 2017. An overview on catalytic hydrodeoxygenation of pyrolysis oil and its model compounds. Catalysts 7 (6), 169. https://doi.org/10.3390/catal7060169.

Silva, N.K.G., Ferreira, R.A.R., Ribas, R.M., et al., 2021. Gas-phase hydrodeoxygenation (HDO) of guaiacol over Pt/Al2O3 catalyst promoted by Nb2O5. Fuel 287, 119509. https://doi.org/10.1016/j.fuel.2020.119509.

Tai, L., Hamidi, R., de Caprariis, B., et al., 2022. Guaiacol hydrotreating with in-situ generated hydrogen over ni/modified zeolite supports. Renew. Energy 182, 647–658. https://doi.org/10.1016/j.renene.2021.10.048.

Tian, Z., Liang, X., Li, R., et al., 2022. Hydrodeoxygenation of guaiacol as a model compound of pyrolysis lignin-oil over NiCo bimetallic catalyst: reactivity and kinetic study. Fuel 308, 122034. https://doi.org/10.1016/j.fuel.2021.122034.

Tran, Q.K., Ly, H.V., Kwon, B., et al., 2021. Catalytic hydrodeoxygenation of guaiacol as a model compound of woody bio-oil over Fe/AC and Ni/γ-Al2O3 catalysts. Renew. Energy 173, 886–895. https://doi.org/10.1016/j.renene.2021.03.138.

Ubando, A.T., Chen, W.H., Tan, R.R., et al., 2020. Optimal integration of a biomass-based polygeneration system in an iron production plant for negative carbon emissions. Int. J. Energy Res. 44 (12), 9350–9366. https://doi.org/10.1002/er.4902.

Wang, H., Lee, S.J., Olarte, M.V., et al., 2016a. Bio-oil stabilization by hydrogenation over reduced metal catalysts at low temperatures. ACS Sustainable Chem. Eng. 4 (10), 5533–5545. https://doi.org/10.1021/acssuschemeng.6b01270.

Wang, J., Wu, Z., Han, L., et al., 2016b. Hollow-structured carbon-supported nickel cobaltite nanoparticles as an efficient bifunctional electrocatalyst for the oxygen reduction and evolution reactions. ChemCatChem 8 (4), 736–742. https://doi.org/10.1002/cctc.201501058.

Wang, Y., Huang, H., Baxter, N.C., et al., 2020. Guaiacol hydrodeoxygenation over Pd catalyst with mesoporous ZSM-5 support synthesized by solid-state crystallization. Catal. Today 358, 60–67. https://doi.org/10.1016/j.cattod.2020.03.009.

Xiang, L., Fan, G., Yang, L., et al., 2021. Structure-tunable pompon-like RuCo catalysts: insight into the roles of atomically dispersed Ru-Co sites and crystallographic structures for guaiacol hydrodeoxygenation. J. Catal. 398, 76–88. https://doi.org/10.1016/j.jcat.2021.04.014.

Yang, M., Zhao, R., Qin, J., et al., 2023. Co-pyrolysis of heavy bio-oil and disposable masks pyrolysate with Ce/Fe-based oxygen carrier catalyst. Fuel 336, 127147. https://doi.org/10.1016/j.fuel.2022.127147.

Yan, P., Kennedy, E., Stockenhuber, M., 2021. Hydrodeoxygenation of guaiacol over BEA supported bimetallic Ni-Fe catalysts with varied impregnation sequence. J. Catal. 404, 1–11. https://doi.org/10.1016/j.jcat.2021.08.033.

Zhang, C., Zhang, Z.C., 2019. Essential quality attributes of tangible bio-oils from catalytic pyrolysis of lignocellulosic biomass. Chem. Rec. 19 (9), 20442–22057. https://doi.org/10.1002/tcr.201900001.

Zhang, H., Yang, C., Tao, Y., et al., 2022. Catalytic cracking of model compounds of bio-oil: characteristics and mechanism research on guaiacol and acetic acid. Fuel Process. Technol. 238, 107512. https://doi.org/10.1016/j.fuproc.2022.107512.

Zhang, M., Hu, Y., Wang, H., et al., 2021. A review of bio-oil upgrading by catalytic hydrotreatment: advances, challenges, and prospects. Mol. Catal. 504, 111438. https://doi.org/10.1016/j.mcat.2021.111438.